The Journal of Chemical Physics ARTICLE scitation.org/journal/jcp

Well-tempered metadynamics applied to field-theoretic simulations of diblock copolymer melts

Cite as: J. Chem. Phys. 157, 114902 (2022); doi: 10.1063/5.0112703
Submitted: 21 July 2022 • Accepted: 21 August 2022 •
Published Online: 19 September 2022

Thomas M. Beardsley and Mark W. Matsen[a)]

AFFILIATIONS

Department of Chemical Engineering, Department of Physics and Astronomy, and Waterloo Institute for Nanotechnology, University of Waterloo, Waterloo Ontario N2L 3G1, Canada

[a)]Author to whom correspondence should be addressed: mwmatsen@uwaterloo.ca

ABSTRACT

Well-tempered metadynamics (WTMD) is applied to field-theoretic simulations (FTS) to locate the order–disorder transition (ODT) in incompressible melts of diblock copolymer with an invariant polymerization index of $\bar{N} = 10^4$. The polymers are modeled as discrete Gaussian chains with $N = 90$ monomers, and the incompressibility is treated by a partial saddle-point approximation. Our implementation of WTMD proves effective at locating the ODT of the lamellar and cylindrical regions, but it has difficulty with that of the spherical and gyroid regions. In the latter two cases, our choice of order parameter cannot sufficiently distinguish the ordered and disordered states because of the similarity in microstructures. The gyroid phase has the added complication that it competes with a number of other morphologies, and thus, it might be beneficial to extend the WTMD to multiple order parameters. Nevertheless, when the method works, the ODT can be located with impressive accuracy (e.g., $\Delta\chi N \sim 0.01$).

I. INTRODUCTION

Field-theoretic simulations (FTS) provide a versatile technique for investigating fluctuation corrections to the self-consistent field theory (SCFT) of block copolymer melts.[1–3] The testing ground for their development has been linear diblocks, where the copolymer consists of a block of fN A-type segments joined to a block of $(1-f)N$ B-type segments. The system is generally modeled as an incompressible melt of continuous Gaussian chains (i.e., elastic threads) with pairwise contact forces between the A and B segments, the strength of which is controlled by the Flory–Huggins χ parameter.[4] Figure 1 shows the SCFT phase diagram[5] for this standard Gaussian-chain model (GCM) in the conformationally symmetric case where the A and B segments have the same statistical length, a. Note that we follow the standard convention of defining segments to have a common volume of ρ_0^{-1}. As originally demonstrated by Fredrickson and Helfand,[6] fluctuation corrections are controlled by the invariant polymerization index, $\bar{N} = a^6\rho_0^2 N$. The main effect of fluctuations is to stabilize the disordered phase, which shifts the order–disorder transition (ODT) to higher χN. The dashed curve in Fig. 1 shows the shift for $\bar{N} = 10^4$,[7] which is close to the upper limit accessible to experiments.[8]

The field-theoretic Hamiltonian for a diblock copolymer melt takes the form[3]

$$\beta H_f[W_-, W_+] = -n \ln Q[W_-, W_+] + \rho_0 \int \left(\frac{\chi_b}{4} + \frac{W_-^2(\mathbf{r})}{\chi_b} - W_+(\mathbf{r}) \right) d\mathbf{r}, \quad (1)$$

where $\beta \equiv k_B T$, n is the total number of molecules, and χ_b controls the bare interaction between A and B segments. $Q[W_-, W_+]$ is the single-chain partition function in a system of non-interacting diblock copolymers, where the A and B segments are acted upon by the external fields $W_+(\mathbf{r}) + W_-(\mathbf{r})$ and $W_+(\mathbf{r}) - W_-(\mathbf{r})$, respectively. Thus, the first term in Eq. (1) is simply the free energy of the non-interacting system in units of $k_B T$, while the second term accounts for the A/B interactions.

In SCFT, the free energy of the melt is approximated by $F = H_f[w_-, w_+]$, where $w_-(\mathbf{r})$ and $w_+(\mathbf{r})$ denote the saddle point

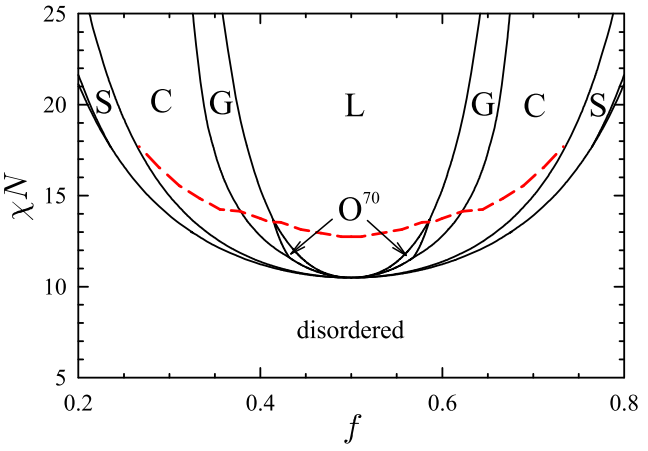

FIG. 1. Phase diagram for conformationally symmetric diblock copolymer melts, calculated using SCFT.[5] The ordered phases are lamellar (L), Fddd (O^{70}), gyroid (G), cylindrical (C), and spherical (S). The dashed curve shows the fluctuation-corrected ODT for $\bar{N} = 10^4$, calculated using FTS.[7]

of the Hamiltonian. The saddle point is obtained by solving the self-consistent conditions $\mathcal{D}H_f/\mathcal{D}W_- = \mathcal{D}H_f/\mathcal{D}W_+ = 0$, where

$$\frac{\beta}{\rho_0}\frac{\mathcal{D}H_f}{\mathcal{D}W_-} = \phi_- + \frac{2}{\chi_b}W_-, \tag{2}$$

$$\frac{\beta}{\rho_0}\frac{\mathcal{D}H_f}{\mathcal{D}W_+} = \phi_+ - 1. \tag{3}$$

Here, $\phi_+(\mathbf{r})$ is the total polymer concentration and $\phi_-(\mathbf{r})$ is the difference between the A and B concentrations (i.e., the composition) in the non-interacting system. In FTS, one instead simulates the field-theoretic Hamiltonian. Note, however, that $W_+(\mathbf{r})$ is imaginary valued, and consequently, $H_f[W_-, W_+]$ is complex valued, which precludes standard simulation techniques.

Lennon *et al.*[9] previously calculated the shift of the ODT using complex Langevin simulations (CL-FTS),[10] where both fields fluctuate in the complex plane. In that work, the ODT was located by evaluating the relative free energy of the ordered and disordered phases using thermodynamic integration (TI). However, the simulations were limited to an unrealistically large value of $\bar{N} = 5.4 \times 10^5$ due to a numerical instability, which poses a potential problem for all complex Langevin simulations.[11] Furthermore, Lennon *et al.* did not account for an ultraviolet (UV) divergence,[9] which occurs as the resolution of the spatial grid used to represent the fields becomes increasingly fine, thereby, in effect, reducing the range of the interactions. In any case, Delaney and Fredrickson[13] have since shown that these TI calculations were, in fact, inaccurate.

Delaney and Fredrickson not only improved the accuracy of the TI but also tamed the instability and removed UV divergence by introducing compressibility and smearing the concentrations (or, equivalently, smearing the interactions). This allowed them to generate a phase diagram for a more realistic $\bar{N} \approx 10^4$. Although the UV divergence was removed, they did not calibrate their interaction parameter to account for the smearing, which is necessary to make quantitative comparisons with the SCFT phase diagram in Fig. 1. Even still, there were qualitative differences with respect to experiments. First, the fluctuation corrections were insufficient to produce direct gyroid–disorder transitions,[8] and second, the fluctuations destroyed the Fddd phase.[14,15] This was likely a result of too much smearing.[2]

An alternative strategy in FTS is to perform a partial saddle-point approximation,[16,17] where $W_-(\mathbf{r})$ fluctuates while $W_+(\mathbf{r})$ follows its saddle point, $w_+(\mathbf{r})$. The rationale is that the composition fluctuations presumably dominate those of the pressure field, and indeed, the approximation appears accurate, at least, for $\bar{N} \gtrsim 10^3$.[2,17,18] An advantage of the partial saddle-point approximation is that $w_+(\mathbf{r})$ is real valued, which allows for the use of standard Langevin simulations (L-FTS),[19] thereby avoiding the instability of CL-FTS. The fluctuation-corrected ODT in Fig. 1 is a result of this particular variant of FTS.[7] Consistent with experiments, L-FTS predict direct gyroid–disorder transitions and a stable Fddd phase.

To avoid the numerical inaccuracies that occur when solving for continuous Gaussian chains, the L-FTS in Ref. 7 modeled the polymers as discrete Gaussian chains. There is no cost of doing so[20] since this modification to the standard GCM can be accounted for, together with the UV divergence, using the Morse calibration of the interaction parameter,

$$\chi = z_\infty \chi_b + c_2\chi_b^2 + c_3\chi_b^3 + \cdots, \tag{4}$$

originally devised for particle-based simulations.[21–24] The first coefficient, z_∞, is the relative number of intermolecular contacts in the limit of $\chi_b \to 0$ and $N \to \infty$, which can be calculated analytically.[3,7,20] The remaining coefficients are determined by fitting the peak of the disordered-state structure function, $S(k^*)$, to renormalized one-loop (ROL) predictions.[25,26] However, for $\bar{N} = 10^4$, the linear approximation, $\chi \approx z_\infty\chi_b$, is reasonably accurate.[3,7]

Although the L-FTS in Ref. 7 produced ODTs consistent with experiments, the simulations were highly computational. Thermodynamic integration was found to be insufficiently accurate, and so the ODT was located by examining the disappearance of Bragg reflections in the ordered-state structure function, $S(k)$, which required a series of long simulations. Here, we demonstrate a more efficient approach using well-tempered metadynamics (WTMD),[27] as previously applied to particle-based simulations.[22,23,28]

II. FIELD-THEORETIC SIMULATIONS

Our FTS follow the implementation in Ref. 7, where the polymers are modeled as discrete chains consisting of N beads (i.e., monomers) connected by springs (i.e., bonds). The first N_A monomers are A-type, and the remaining $N_B = N - N_A$ monomers are B-type, resulting in a composition of $f = N_A/N$. The bonds are harmonic with a statistical length of a such that the unperturbed end-to-end length of the entire polymer is $R_0 = a\sqrt{N}$ in the large-N limit. Although the monomers are treated as point particles, they are each assigned a finite volume of ρ_0^{-1}. Thus, the total number of polymers is given by

$$n = \frac{\rho_0 V}{N} = \frac{V}{R_0^3}\sqrt{\bar{N}}, \tag{5}$$

where V is the volume of the system. The simulations are generally conducted in an $L_x \times L_y \times L_z$ orthorhombic box with periodic

boundary conditions. All spatially dependent quantities are specified at the vertices of an $m_x \times m_y \times m_z$ grid with a regular spacing of $\Delta_\alpha = L_\alpha/m_\alpha$ in each direction α. Hence, the system has a total volume of $V = L_x L_y L_z$, while each grid point corresponds to a volume of $V_{\text{cell}} = \Delta_x \Delta_y \Delta_z$.

The statistical mechanics of the non-interacting system requires a partial partition function, $q_i(\mathbf{r})$, for the first i monomers of a discrete chain with its ith monomer constrained to position $\mathbf{r}$. It satisfies the recursion relation

$$q_{i+1}(\mathbf{r}) = h_{i+1}(\mathbf{r}) \int g(R) q_i(\mathbf{r} - \mathbf{R}) d\mathbf{R}, \tag{6}$$

subject to the initial condition $q_1(\mathbf{r}) = h_1(\mathbf{r})$.[29] Here,

$$g(R) = \left(\frac{3}{2\pi a^2}\right)^{3/2} \exp\left(-\frac{3R^2}{2a^2}\right) \tag{7}$$

is a Boltzmann weight for the bond potential and

$$h_i(\mathbf{r}) = \exp(-W_+(\mathbf{r}) - \gamma_i W_-(\mathbf{r})) \tag{8}$$

is a Boltzmann weight for the field acting on the ith monomer, where $\gamma_i = 1$ for $i \le N_A$ and $\gamma_i = -1$ otherwise. The calculation also requires an analogous partial partition function, $q_i^\dagger(\mathbf{r})$, for the last $N + 1 - i$ monomers of the chain, which is obtained by iterating

$$q_{i-1}^\dagger(\mathbf{r}) = h_{i-1}(\mathbf{r}) \int g(R) q_i^\dagger(\mathbf{r} - \mathbf{R}) d\mathbf{R}, \tag{9}$$

starting from $q_N^\dagger(\mathbf{r}) = h_N(\mathbf{r})$. The recursion relations are solved using fast Fourier transforms.[7]

Once both partial partition functions have been obtained, the single-chain partition function is given by

$$Q[W_-, W_+] = \frac{1}{V} \int \frac{q_i(\mathbf{r}) q_i^\dagger(\mathbf{r})}{h_i(\mathbf{r})} d\mathbf{r}, \tag{10}$$

which is, in fact, independent of i. We also require the composition and total concentration in the non-interacting system, which are given by

$$\phi_-(\mathbf{r}) = \frac{1}{NQ} \sum_{i=1}^{N} \gamma_i \frac{q_i(\mathbf{r}) q_i^\dagger(\mathbf{r})}{h_i(\mathbf{r})}, \tag{11}$$

$$\phi_+(\mathbf{r}) = \frac{1}{NQ} \sum_{i=1}^{N} \frac{q_i(\mathbf{r}) q_i^\dagger(\mathbf{r})}{h_i(\mathbf{r})}, \tag{12}$$

respectively.

In L-FTS, the composition field fluctuates according to the dynamics

$$W_-(\mathbf{r}; \tau + \delta\tau) = W_-(\mathbf{r}; \tau) - \frac{\beta}{\rho_0} \frac{\mathcal{D}H_f}{\mathcal{D}W_-(\mathbf{r})} \delta\tau + \mathcal{N}(0, \sigma_\tau), \tag{13}$$

where τ is the simulation time and $\mathcal{N}(0, \sigma_\tau)$ provides a random number generated from a normal distribution of zero mean and $\sigma_\tau^2 = 2\delta\tau/\rho_0 V_{\text{cell}}$ variance. To improve accuracy, we apply the predictor-corrector algorithm,[19,30] and to maximize computational speed, we use a reasonably optimized time step of $\delta\tau = 1/N$.[7] After each time step, $w_+(\mathbf{r})$ is adjusted using Anderson mixing[3,31] to enforce $\mathcal{D}H_f/\mathcal{D}W_+ = 0$. We note that during the preparation of our paper, Yong and Kim[32] published a more efficient method of adjusting $w_+(\mathbf{r})$ that uses machine learning.

III. WELL-TEMPERED METADYNAMICS

Previous studies have located the ODT by monitoring a collective variable or order parameter, Ψ, but the accuracy was limited by metastability.[33,34] Well-tempered metadynamics (WTMD)[27,35,36] overcomes the energy barriers separating the two phases by adding a biasing potential, $U(\Psi)$, to the Hamiltonian. The resulting Hamiltonian,

$$H = H_f + U(\Psi), \tag{14}$$

is then simulated by adding

$$\frac{\mathcal{D}U}{\mathcal{D}W_-(\mathbf{r})} = U'(\Psi) \frac{\mathcal{D}\Psi}{\mathcal{D}W_-(\mathbf{r})} \tag{15}$$

to the forcing term in Eq. (13).

For WTMD to perform well, one needs to devise an effective order parameter, which is typically constructed by experimenting with various options. Morse and co-workers[22,23,28] described the rationale by which they settled on a weighted ℓ-norm of the Fourier transform of the composition. Here, we convert their particle-based order parameter to a field-based version,

$$\Psi = \frac{1}{R_0^3} \left(\frac{V}{(2\pi)^3} \int f(k) |W_-(\mathbf{k})|^\ell d\mathbf{k} \right)^{\frac{1}{\ell}}, \tag{16}$$

involving the Fourier transform of the composition field,

$$W_-(\mathbf{k}) = \mathcal{F}[W_-(\mathbf{r})] = \int W_-(\mathbf{r}) e^{i\mathbf{k}\cdot\mathbf{r}} d\mathbf{r}. \tag{17}$$

Morse and co-workers experimented with different norms, but found that the $\ell = 4$ one performed best. They also found it useful to screen out the large wavevector contributions by selecting a weighting function of

$$f(k) = \frac{1}{1 + \exp(12(k/k_c - 1))}. \tag{18}$$

Following their recommendation, we set k_c to 1.4 times the peak position of the disordered-state structure function, $S(k)$. For this particular order parameter, the functional derivative in Eq. (15) is given by

$$\frac{\mathcal{D}\Psi}{\mathcal{D}W_-(\mathbf{r})} = \frac{V R_0^{3(\ell-1)}}{\Psi^{\ell-1}} \mathcal{F}^{-1}\left[f(k) |W_-(\mathbf{k})|^{\ell-2} W_-(\mathbf{k}) \right]. \tag{19}$$

A WTMD simulation generally begins with $U(\Psi) = 0$. Once the system has equilibrated, Gaussians,

$$\beta\delta U(\Psi) = \exp\left(-\frac{U(\Psi)}{k_B\Delta T}\right)\exp\left(-\frac{(\hat{\Psi}-\Psi)^2}{2\sigma_\Psi^2}\right), \tag{20}$$

are periodically added to $U(\Psi)$ centered about the instantaneous value of the order parameter, $\hat{\Psi}$. The width of the Gaussians, σ_Ψ, needs to be large enough that $U(\Psi)$ remains reasonably smooth but not so much so as to smear the relevant features. Although the rate at which Gaussians are added becomes irrelevant in the long-time limit,[27] it should be sufficiently slow for Ψ to migrate a distance of σ_Ψ between the addition of Gaussians. We find that 10^3 Langevin steps work well. In well-tempered metadynamics, the amplitude of the Gaussians gradually shuts off at a rate controlled by ΔT. Although the method is robust with respect to the exact choice, $k_B\Delta T$ should ideally be similar in size to the energy barrier separating the two phases.[27] Note that the functional derivative of $U(\Psi)$ in Eq. (15) requires $U'(\Psi)$, and therefore, we also update it along with $U(\Psi)$ using

$$\delta U'(\Psi) = \left(\frac{\hat{\Psi}-\Psi}{\sigma_\Psi^2} - \frac{U'(\Psi)}{k_B\Delta T}\right)\delta U(\Psi). \tag{21}$$

Once the system has reached a well-tempered state, the free energy as a function of the order parameter is given by[27]

$$F(\Psi;\chi_b) = -\frac{T+\Delta T}{\Delta T}U(\Psi) + \text{constant}. \tag{22}$$

A histogram of the order parameter can then be calculated using

$$P(\Psi) \propto \exp(-\beta F(\Psi;\chi_b)), \tag{23}$$

which typically produces two peaks, one for each phase. The stable phase corresponds to the peak with the largest probability, and thus, the phase transition is located by adjusting χ_b until the areas under the two peaks are equal. Provided that the transition is sufficiently close to χ_b of the simulation, the change in free energy can be approximated by the linear extrapolation,

$$F(\Psi;\chi_b+\Delta\chi_b) = F(\Psi;\chi_b) + \frac{\partial F}{\partial\chi_b}\Delta\chi_b, \tag{24}$$

used by Ghasimakbari and Morse.[28] The partial derivative of the free energy is evaluated during the WTMD simulation using

$$\frac{\partial F}{\partial\chi_b} = \left\langle\frac{\partial H}{\partial\chi_b}\right\rangle_\Psi = \frac{\rho_0 V}{4\beta} - \frac{\rho_0}{\beta\chi_b^2}\left\langle\int W_-^2(\mathbf{r})d\mathbf{r}\right\rangle_\Psi, \tag{25}$$

where the partial derivative of the Hamiltonian is averaged over the configurations of a particular Ψ value. To create a smooth derivative, we construct two functions, $I_0(\Psi)$ and $I_1(\Psi)$, in an analogous manner to $U(\Psi)$. At each $\hat{\Psi}$, we add a Gaussian to $I_0(\Psi)$ and a Gaussian weighted by $\int W_-^2(\mathbf{r})d\mathbf{r}$ to $I_1(\Psi)$. At the end of the simulation, the ensemble average in Eq. (25) is approximated by $I_1(\Psi)/I_0(\Psi)$.

IV. RESULTS

Our previous study[7] estimated the ODT for $\bar{N} = 10^4$ (dashed curve in Fig. 1) by locating the points where the Bragg reflections in the ordered-state structure function, $S(k)$, vanish. The method is highly computational, and furthermore, it is prone to inaccuracies due to the metastability of the ordered phases. Here, we test the WTMD method on four of the compositions corresponding to the lamellar (L), cylindrical (C), spherical (S), and gyroid (G) phases. As before, we use the linear approximation $\chi = z_\infty\chi_b$, given the large value of $\bar{N}$.

A. Lamellar–disorder transition

For the L–dis transition, we select a composition of $N_A = 40$ and $N_B = 50$. Our previous study found an ODT of $(\chi N)_{\text{ODT}} = 13.15 \pm 0.05$ in a cubic simulation box of size $L = 4.38R_0$, which was optimized for three lamellar periods. The fields were represented on a $40 \times 40 \times 40$ grid, for which the ratio of the effective and bare interaction parameters is $z_\infty = 0.767$.

Using these same conditions, we perform WTMD with the $\ell = 4$ version of the order parameter used by Morse and

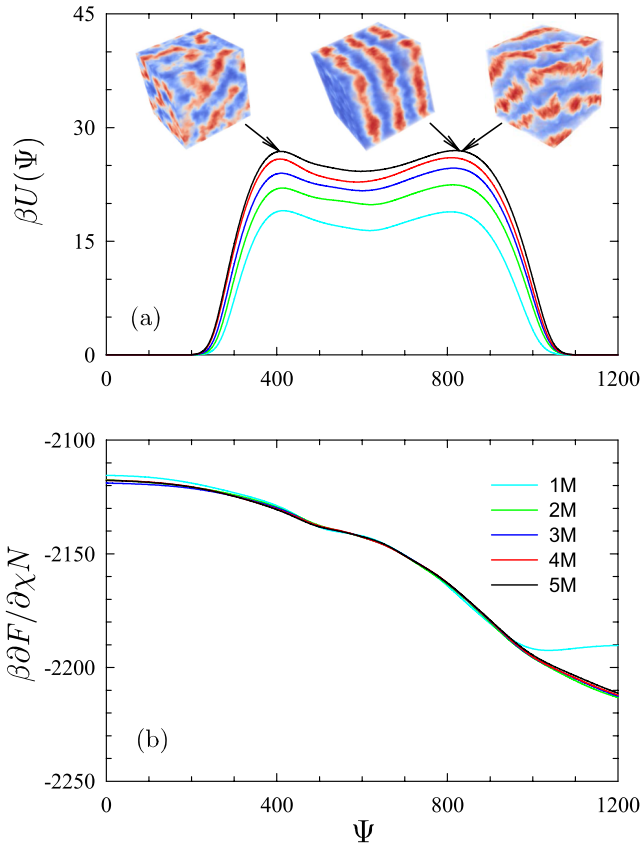

FIG. 2. (a) Bias potential, $U(\Psi)$, and (b) derivative of the free energy, $\partial F(\Psi;\chi)/\partial\chi$, from a WTMD simulation for $N_A = 40$, $N_B = 50$, and $\chi N = 13.15$. Both quantities are plotted after every 10^6 Langevin steps. The insets in (a) show sample configurations from the two peaks of $U(\Psi)$.

co-workers.[22,23,28] On the basis of several trial runs, the disordered and lamellar phases occur at $\Psi \approx 400$ and 800, respectively, and they are separated by an energy barrier of about $5k_BT$. Guided by these findings, we perform a long WTMD simulation of 5×10^6 Langevin steps with $\sigma_\Psi = 40$ and $\Delta T/T = 5$. Figure 2 shows the resulting bias potential, $U(\Psi)$, and free energy derivative, $\partial F/\partial\chi$, after every 10^6 steps. The bias potential quickly develops two peaks matching the expected positions, and visual inspection of the configurations (see the insets) confirms that the peaks do, indeed, correspond to the disordered and lamellar phases. Note that the lamellae form in either the (300) or (221) orientation, both of which result in the same lamellar period of $D = L/3$. Although we perform 5×10^6 steps, the shape of $U(\Psi)$ and the derivative $\partial F/\partial\chi$ are reasonably accurate after the first 10^6 steps.

Figure 3(a) plots the histogram of the order parameter as the number of Langevin steps increases. Even though the shape of $U(\Psi)$ is relatively static after 10^6 steps, the histogram continues to fluctuate significantly. Nevertheless, when extrapolated to the point where the two peaks have equal areas (i.e., the ODT), the resulting histogram shown in Fig. 3(b) is also relatively static. Furthermore, the extrapolated values of χN plotted in the inset are nicely consistent with an ODT of $(\chi N)_{\text{ODT}} = 13.14 \pm 0.01$. Not only does this match our previous estimate using $S(k)$, but also this new estimate from WTMD is much more precise.

Given that χN of our simulation and that of the projected ODT differ by only 0.01, Fig. 3 does not provide a particularly compelling test of the extrapolation in Eq. (24). Therefore, we run two more WTMD simulations, one below the ODT at $\chi N = 13.11$ and another above at $\chi N = 13.19$. Figure 4(a) compares the resulting histograms, $P(\Psi)$, to that of $\chi N = 13.15$. The comparison illustrates that the histograms are exceptionally sensitive to the value of χN, which bodes well for the potential accuracy of the method. Figure 4(b) then extrapolates the three histograms to the point where their peaks have equal areas. The agreement among the resulting histograms and among the corresponding estimates of $(\chi N)_{\text{ODT}}$ plotted in the inset confirm that the extrapolation works well.

Our previous estimates of the ODT based on the structure function, $S(k)$, found that the optimum size of the simulation box is ~1%

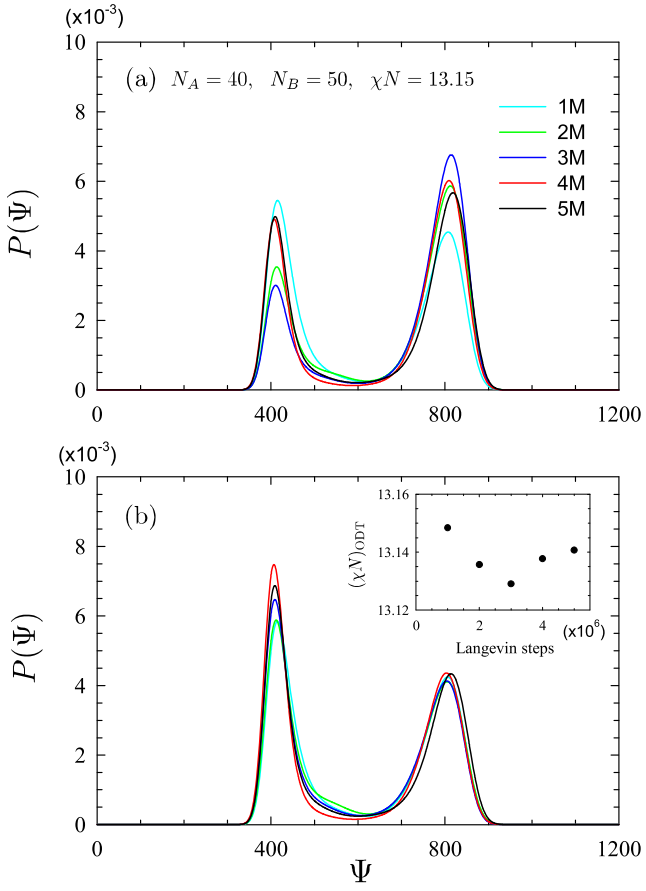

FIG. 3. Histogram of the order parameter, $P(\Psi)$, at (a) the $\chi N = 13.15$ of the simulation and (b) the estimated $(\chi N)_{\text{ODT}}$ plotted in the inset as the number of Langevin steps is increased.

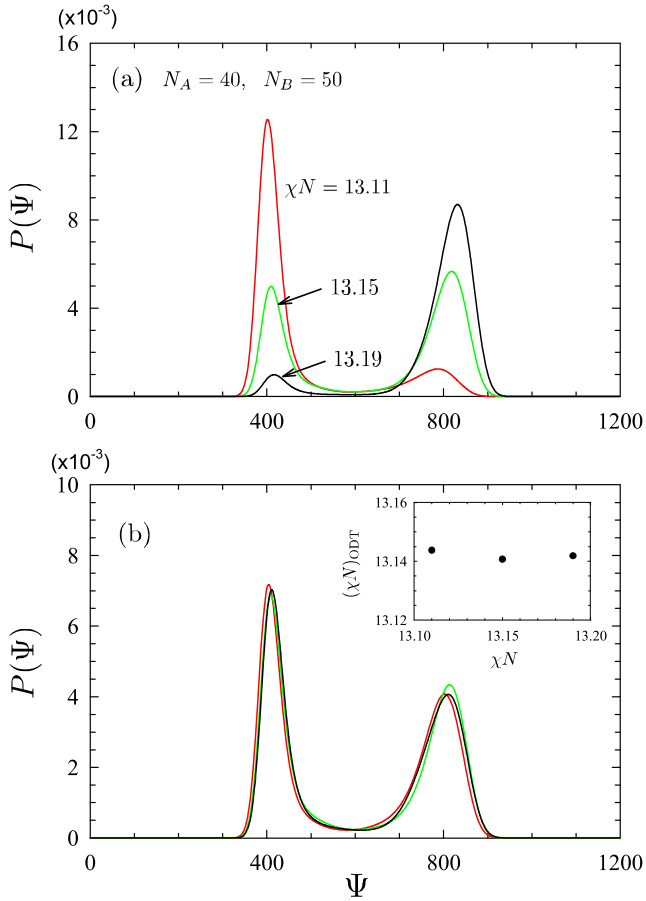

FIG. 4. Histograms of the order parameter, $P(\Psi)$, from three different simulations plotted at (a) the χN of the run and (b) the estimated $(\chi N)_{\text{ODT}}$ shown in the inset.

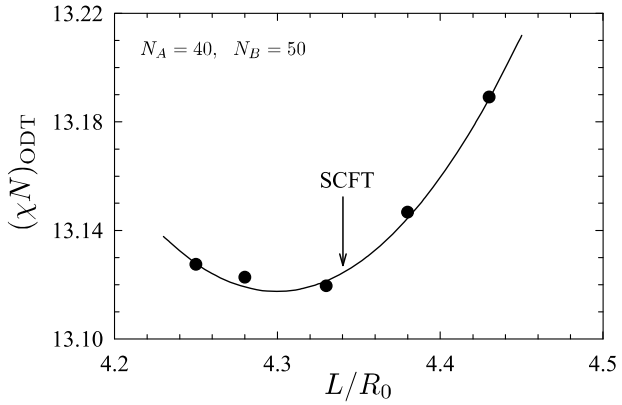

FIG. 5. ODT estimates for different box sizes (symbols) fit to a parabola (solid curve). The arrow denotes three times the equilibrium lamellar period predicted by SCFT at $\chi N = 13.12$.

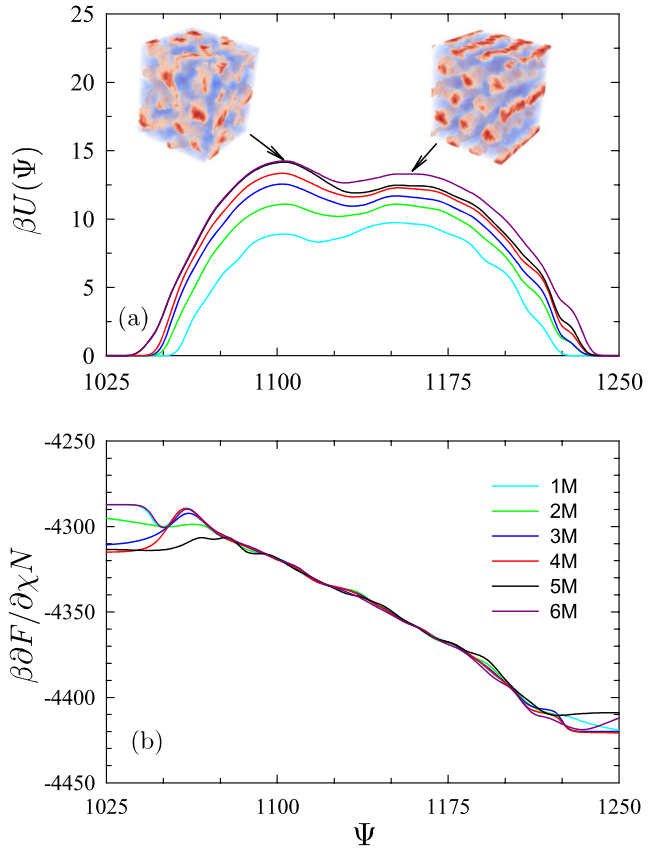

FIG. 6. (a) Bias potential, $U(\Psi)$, and (b) derivative of the free energy, $\partial F(\Psi; \chi)/\partial\chi$, from a WTMD simulation for $N_A = 30$, $N_B = 60$, and $\chi N = 14.85$. Both quantities are plotted after every 10^6 Langevin steps. The insets in (a) show sample configurations from the two peaks of $U(\Psi)$.

larger than the SCFT prediction.[7] We now repeat the optimization with WTMD by calculating $(\chi N)_{\rm ODT}$ for a range of different box sizes. Disregarding small boxes exhibiting occasional instances of the (220) orientation and large boxes exhibiting the (310) orientation, Fig. 5 plots the ODTs from the simulations that only formed (300) and (221) lamellar orientations. The solid curve denotes a parabolic fit, which provides a more accurate ODT of $(\chi N)_{\rm ODT} = 13.12 \pm 0.01$, corresponding to an optimum box size of $L = 4.30R_0$. This time, the optimum box size is about 1% smaller than the three lamellar periods of SCFT ($D_{\rm SCFT} = 1.448R_0$).

B. Cylindrical–disorder transition

We now turn our attention to the C–dis transition for $N_A = 30$ and $N_B = 60$. Our previous study estimated an ODT of $(\chi N)_{\rm ODT} = 14.85 \pm 0.05$. That study used a simulation box with a cross-sectional area of $4.78R_0 \times 5.52R_0$, optimized for six unit cells, and a longer dimension in the direction of the cylinder axes. In WTMD simulations, the cylinders need to form spontaneously. To help facilitate this, we set $L_x = L_y = 4.78R_0$ and $L_z = 5.52R_0$, which should allow the cylinders to form in either the x or y direction. The fields are represented on a $48 \times 48 \times 48$ grid, for which $z_\infty = 0.752$.

Figure 6(a) shows the resulting bias potential from a WTMD simulation at $\chi N = 14.85$ after every 10^6 Langevin steps for parameters of $\ell = 4$, $\sigma_\Psi = 4$, and $\Delta T/T = 2.5$. Again, there are two peaks, one at $\Psi \approx 1100$ corresponding to disordered configurations and another at $\Psi \approx 1160$ corresponding to ordered cylinders (see the insets). As expected, the ordered phase switches between cylinders in the x and y directions. This time, it takes about 2×10^6 steps for the shape of $U(\Psi)$ to converge, but, nevertheless, we continue the simulation for 6×10^6 steps. The derivative $\partial F/\partial\chi$, shown in Fig. 6(b), is reasonably accurate after 10^6 steps, apart from the extremes, which are not important.

Figure 7(a) plots the histogram, $P(\Psi)$, as the number of time steps increases. As mentioned before, the relative size of the two peaks fluctuates significantly with time. Nevertheless, the extrapolation of the histogram to equal-sized peaks, plotted in Fig. 7(b), is well converged after 3×10^6 Langevin steps. From the extrapolated values of χN shown in the inset, we obtain an ODT of $(\chi N)_{\rm ODT} = 14.87 \pm 0.01$. Again, this is consistent with and more precise than our previous estimate based on $S(k)$.

C. Spherical–disorder transition

Next, we consider the S–dis transition for $N_A = 24$ and $N_B = 66$. From the disappearance of Bragg reflections in $S(k)$, our previous study estimated an ODT of $(\chi N)_{\rm ODT} = 18.05 \pm 0.05$. Those simulations were conducted in a cubic box of size $L = 5.71R_0$, which was optimized for 27 bcc unit cells. The grid was set to $48 \times 48 \times 48$, which leads to $z_\infty = 0.790$.

In this case, the $\ell = 2$ version of the order parameter in Eq. (16) is found to be more effective than the $\ell = 4$ version in distinguishing the ordered and disordered phases. As demonstrated in Fig. 8(a), there is still relatively little separation between the $\Psi \approx 7.15$ of the disordered phase at $\chi N = 18.0$ and the $\Psi \approx 7.35$ of the spherical phase at $\chi N = 18.1$. The lack of separation does not bode

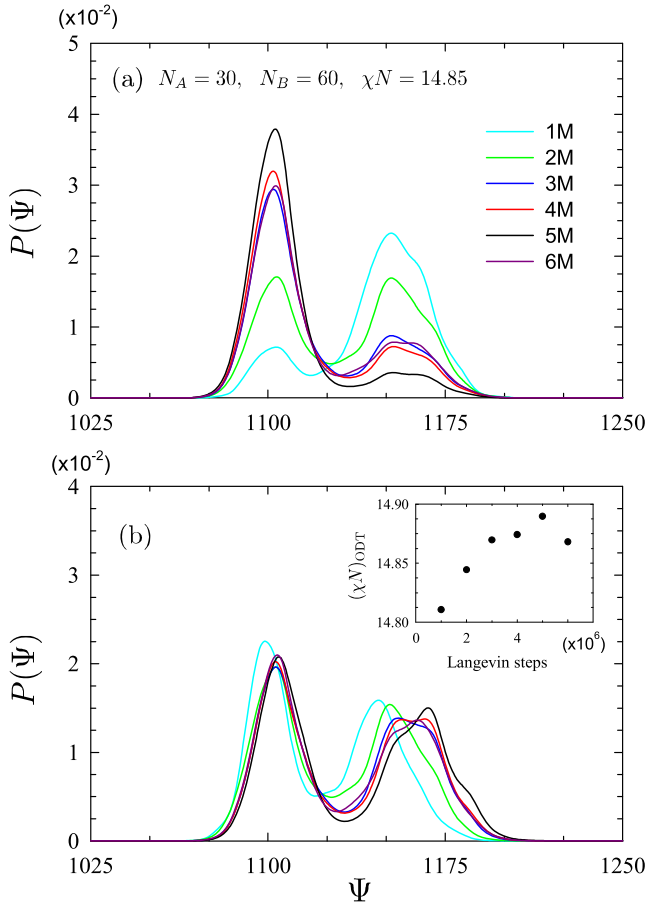

FIG. 7. Histogram of the order parameter, $P(\Psi)$, at (a) the $\chi N = 14.85$ of the simulation and (b) the estimated $(\chi N)_{ODT}$ plotted in the inset as the number of Langevin steps is increased.

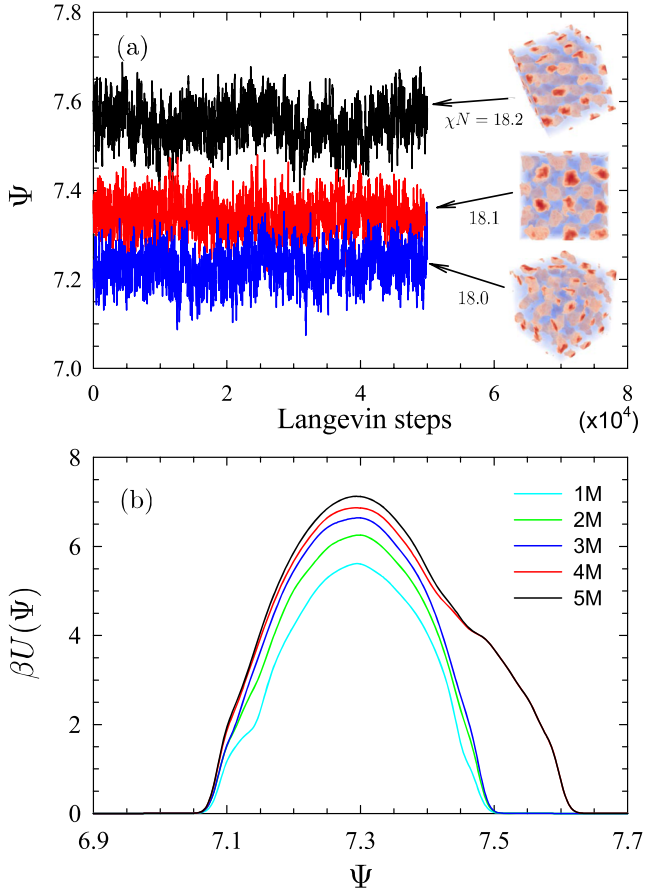

FIG. 8. (a) Order parameters of the disordered, S, and C phases for $N_A = 24$ and $N_B = 66$ during FTS at $\chi N = 18.0$, 18.1, and 18.2, respectively. (b) Bias potential, $U(\Psi)$, after every 10^6 Langevin steps during a WTMD simulation at $\chi N = 18.05$.

well for WTMD, but, nevertheless, we attempt a WTMD simulation at $\chi N = 18.05$ using $\sigma_\Psi \approx 0.015$ and $\Delta T/T = 1$. As suspected, the bias potential, $U(\Psi)$, plotted in Fig. 8(b) fails to generate separate peaks for the spherical and disordered phases. Interestingly though, $U(\Psi)$ develops a shoulder at $\Psi \approx 7.6$ after 2×10^6 Langevin steps. Visual inspection of the configurations reveals cylindrical minority domains.

Our previous study[7] had, in fact, observed an epitaxial C ↔ S transition[37] at $(\chi N)_{OOT} = 18.15 \pm 0.05$. Indeed, Fig. 8(a) confirms that the position of the shoulder coincides with the average value of Ψ obtained from the cylindrical phase at $\chi N = 18.2$. To locate the order–order transition, we run two additional WTMD simulations at $\chi N = 18.15$ and 18.2. Given the larger separation between the C and S phases, we increase the width of the Gaussians to $\sigma_\Psi = 0.04$. The resulting biases plotted in Fig. 9 illustrate that S is still favored at the lower segregation, but C becomes more stable at the higher segregation. Extrapolations predict $(\chi N)_{OOT} = 18.17 \pm 0.01$, which is again consistent with and more accurate than the estimate based on $S(k)$.[7]

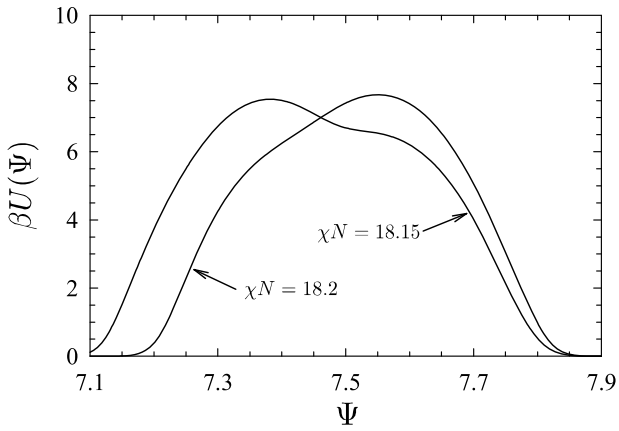

FIG. 9. Bias potentials, $U(\Psi)$, bracketing the epitaxial C ↔ S transition for $N_A = 24$ and $N_B = 66$.

D. Gyroid–disorder transition

We conclude our study by testing WTMD on the G–dis transition for $N_A = 36$ and $N_B = 54$. Our previous study estimated an ODT of $(\chi N)_{\rm ODT} = 13.75 \pm 0.05$ using a simulation box optimized for eight unit cells. However, this is too large for the gyroid phase to spontaneously form within a reasonable simulation time, and so we reduce the box to an optimal size, $L = 3.689R_0$, for one unit cell and set the grid to $32 \times 32 \times 32$, for which $z_\infty = 0.782$. Naturally, this will amplify finite-size effects, potentially shifting the ODT to some degree. Therefore, we repeat the simulations in Ref. 7, where χN is reduced until the Bragg reflections of the G phase vanish. As evident from Fig. 10, the transition for the smaller system does occur at a slightly reduced $(\chi N)_{\rm ODT} = 13.55 \pm 0.05$.

As was the case for the S–dis transition, the $\ell = 2$ version of Ψ plotted in Fig. 11(a) is better able to distinguish the gyroid and disordered phases. Even still, the separation in Ψ is again relatively small. Indeed, the bias potential plotted in Fig. 11(b) for a WTMD simulation at $\chi N = 13.55$ with $\sigma_\Psi \approx 0.025$ and $\Delta T/T = 1$ fails to produce distinct peaks for the ordered and disordered phases. The problem this time, however, is somewhat more complicated. Not only are the ordered and disordered phases similar in structure, but also visual inspection of the configurations reveals that there are other morphologies competing for stability.

Figure 12 shows the evolution of the order parameter during the WTMD simulation with the different morphologies identified every 5×10^4 Langevin steps. In addition to the gyroid phase, we observe a cylindrical phase, a perforated-lamellar phase, and an Fddd-like phase. Although a true Fddd phase requires a non-cubic simulation box of specific dimensions, the system is, nevertheless,

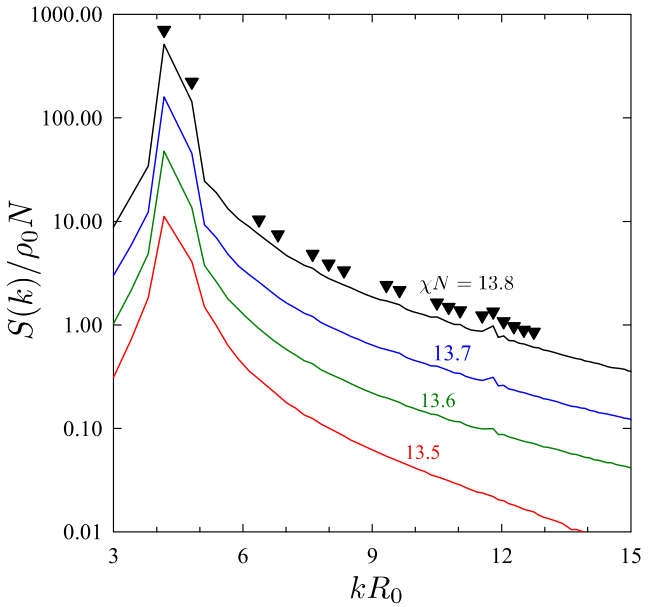

FIG. 10. Structure function, $S(k)$, at a sequence of χN values, calculated for $N_A = 36$ and $N_B = 54$. For clarity, the curves for the ordered state, exhibiting the Bragg peaks, are shifted up by factors of 3. The triangles denote the allowed peak positions for the Ia3d symmetry.

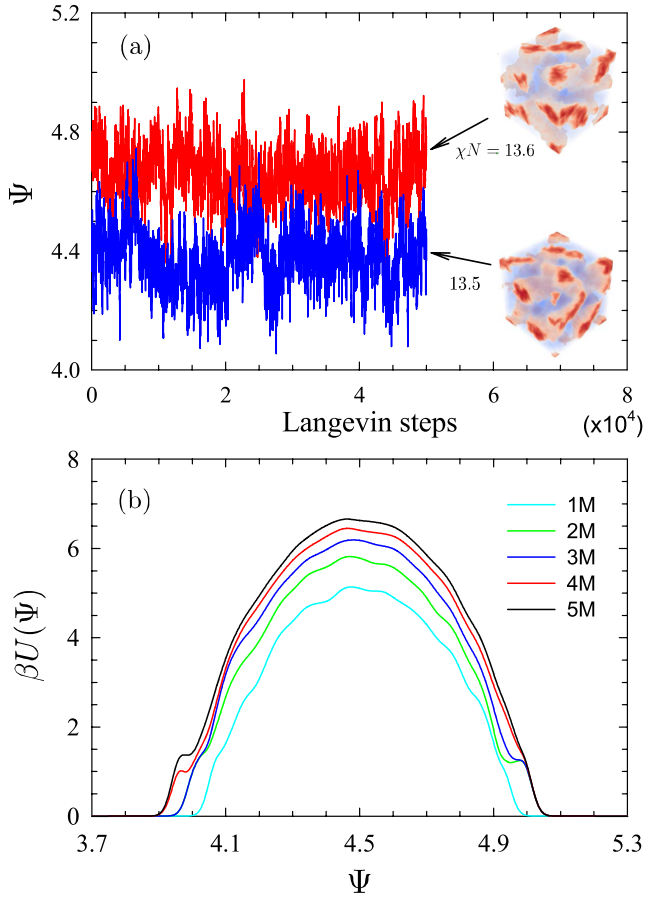

FIG. 11. (a) Order parameters of the disordered and G phases for $N_A = 36$ and $N_B = 54$ during FTS at $\chi N = 13.5$ and 13.6, respectively. (b) Bias potential, $U(\Psi)$, after every 10^6 Langevin steps during a WTMD simulation at $\chi N = 13.55$.

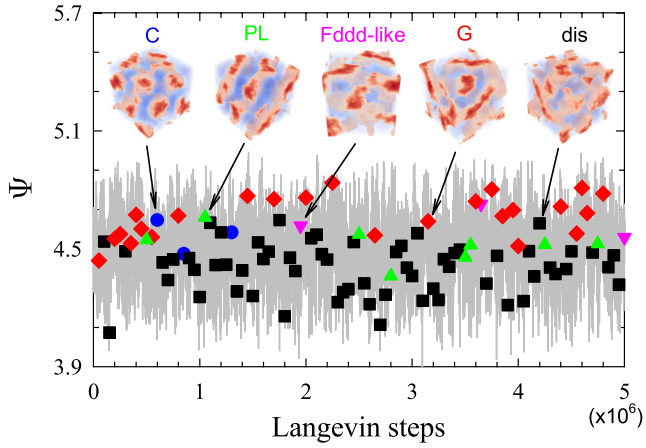

FIG. 12. Evolution of the order parameter in the WTMD simulation of Fig. 11. The symbols denote the observed morphology every 5×10^4 Langevin steps.

able to form a similar network-structure in cubic boxes, as was the case in our previous study.[7]

V. DISCUSSION

The previous ODT calculations in Ref. 7 are accurate to within the linewidths in Fig. 1, and our new calculations are even more precise. The impressive accuracy of WTMD can be attributed to the fact that the histogram of the order parameter, $P(\Psi)$, is highly sensitive to χ, as illustrated in Fig. 4(a). Consequently, however, the method needs to be performed close to the actual transition. Here, we had accurate estimates of the ODTs from our previous simulations in Ref. 7. In the absence of such estimates, it is advisable to first run scans back and forth across the ODT while monitoring the order parameter. Not only will the hysteresis loop bracket the ODT, but also the scans will provide values of the order parameter in the disordered and ordered phases, which can then guide the choice of σ_Ψ. Prior to simulation, one does not generally know the size of the energy barrier separating the two phases to guide the choice of ΔT, but fortunately, WTMD is not particularly sensitive to its value. In any case, it is best to underestimate its optimum value, and then, if necessary, stop and restart the run with a larger ΔT keeping the previous $U(\Psi)$. The initialization of $U(\Psi)$ is arbitrary,[27] but the simulation does need to run long enough to adequately sample the relevant range of Ψ. This will generally happen more quickly if ΔT is increased rather than decreased.

Previous studies[7,11,19,34] have demonstrated that the periodicity of the L and C phases can be determined by comparing the stresses,

$$\sigma_\alpha = \frac{L_\alpha}{Q}\frac{\partial Q}{\partial L_\alpha}, \tag{26}$$

in the $\alpha = x$, y, and z directions, but this does not work for triply periodic phases. Fortunately, though, there is now strong evidence that SCFT provides an accurate estimate of the equilibrium periodicity in FTS,[19,34] which incidentally also appears to be the case for particle-based simulations.[23,28,38,39] Our results in Fig. 5 not only support this but also illustrate that the resulting inaccuracy in the periodicity has little effect on the estimated value of $(\chi N)_{\mathrm{ODT}}$. However, the SCFT requires an accurate value of the effective χ, and thus, one may need to perform the non-linear calibration in Eq. (4) for smaller values of $\tilde{N}$. We note that Delaney and Fredrickson[11,13] found a similar agreement between CL-FTS and SCFT for the lamellar period, but this is not equivalent. The former examples involve comparisons to SCFT predictions of the standard GCM evaluated at the effective χ, whereas the agreement observed by Delaney and Fredrickson is for the SCFT of their modified model evaluated at the bare χ_b.

The challenge with WTMD is finding an order parameter capable of distinguishing the competing phases. Fortunately, there is a sufficient change in the morphology when the L and C phases disorder. Likewise, the order parameter in Eq. (16) is able to adequately distinguish the C and S phases. However, as illustrated by the insets in Fig. 8(a), the morphology of the S phase is too similar to its disordered counterpart. Both are composed of spherical minority domains, but in one case, the domains are arranged in a bcc lattice, while in the other case, they are simply disordered. To overcome this problem, one would need to devise an alternative order parameter that is more sensitive to the periodic arrangement of spheres (i.e., the Bragg reflections in the structure function), which might be a suitable task for machine learning.[36] Note, however, that the method would also need to provide the derivative of Ψ with respect to $W_-(\mathbf{r})$ for the Langevin dynamics. Although this necessity could be avoided by switching to Monte Carlo dynamics, this would greatly reduce the efficiency of simulations.[19]

The G–dis transition possesses the same problem in that the ordered network structure of the G phase transforms into a similar disordered network that simply lacks any long-range order. However, in addition to this, G competes with other network phases (e.g., PL and Fddd) exhibiting similar values of the order parameter. Consequently, our bias was unable to separate the competing phases. Again, this could be remedied by an order parameter that is more sensitive to crystalline symmetry, but it might also help to extend the WTMD to multiple order parameters.[36]

Provided that the order parameter can adequately discern the competing phases, WTMD is able to locate the ODT with remarkable precision. Not only are its predictions consistent with and more accurate than the previous ones obtained from $S(k)$,[7] but also the computational cost is much lower. The previous method requires multiple long simulations of $S(k)$, and furthermore, it has a tendency to underestimate $(\chi N)_{\mathrm{ODT}}$ due to the metastability of ordered phases. This could be problematic at smaller values of $\tilde{N}$, where the first-order nature of the ODT is stronger, allowing for greater degrees of superheating. On the other hand, WTMD can readily cope with large energy barriers by simply increasing ΔT. In fact, larger energy barriers produce narrower peaks in $P(\Psi)$, making it easier to discern the transition.

In our previous study,[7] we had difficulty locating the ODT using thermodynamic integration (TI).[9,40] We did, however, manage to find a L–dis transition for symmetric $N_A = N_B = 45$ diblocks at $(\chi N)_{\mathrm{ODT}} = 12.68$, which compares well with the accurate $(\chi N)_{\mathrm{ODT}} = 12.71 \pm 0.01$ from a WTMD simulation (not shown). To achieve this level of agreement, the TI had to evaluate the free energies of the lamellar and disordered phases, F_L and F_{dis}, to an accuracy of $\pm 10^{-4} nk_BT$, which required a relative accuracy of one part in 10^4 for the free energy derivatives used in the TI. At asymmetric compositions, where the ordered and disordered phases are less distinct, the relative accuracy would need to be even greater.

Fredrickson and Delaney[11] have recently proposed a direct method of evaluating the free energy, which is much less computational than TI. The method is based on the identity

$$F = L_\alpha \frac{\partial F}{\partial L_\alpha} - V L_\alpha \frac{\partial}{\partial L_\alpha}\left(\frac{F}{V}\right). \tag{27}$$

Assuming the thermodynamic limit (i.e., $F \propto V$), the second derivative can be neglected, and thus, the free energy can be approximated by

$$F = L_\alpha \left\langle \frac{\partial H_f}{\partial L_\alpha} \right\rangle, \tag{28}$$

where the derivative of F is obtained by averaging the derivative of H_f from a FTS. To test this expression, we evaluate the free energies of the lamellar and disordered phases for symmetric diblocks at $\chi N = 12.71$, where we would expect $F_L = F_{\mathrm{dis}}$. To account for the UV divergence, we remove its free energy contribution,

$$F_{\mathrm{UV}} = -\frac{Mk_BT}{2}\ln\left(\frac{\chi_b M}{V\rho_0}\right), \tag{29}$$

from the Hamiltonian (i.e., $H_f \to H_f - F_{\mathrm{UV}}$) and differentiate H_f at constant effective χ.[41] The resulting free energies are $F_L = 3.1368\, nk_BT$ and $F_{\mathrm{dis}} = 3.1349\, nk_BT$. A linear extrapolation of the free energies using the derivatives from Ref. 7 gives $(\chi N)_{\mathrm{ODT}} = 12.95$. Although this is a reasonable estimate of the ODT, it is less accurate than the one from TI. Unlike TI where there are only statistical and numerical inaccuracies, this direct method of calculating free energy has additional inaccuracies resulting from its reliance on the assumptions that $F \propto V$ and $\chi = z_\infty \chi_b$.

In reality, order–disorder transitions, particularly the S–dis and G–dis ones, will be challenging to locate for any method based on either order parameters or free energies. However, we expect this to be the exception rather than the rule. For most transitions, the morphologies of the competing phases will have distinguishing characteristics that can be readily discerned by an appropriate order parameter. Indeed, we have started applying WTMD to block copolymer blends in a grand-canonical ensemble using the blend composition as the order parameter, and it is working exceptionally well.

VI. SUMMARY

Well-tempered metadynamics (WTMD) was applied to field-theoretic simulations (FTS) to locate order–disorder transitions (ODTs) of AB diblock copolymer melts with an invariant polymerization index of $\bar{N} = 10^4$. The simulations modeled the polymers as chains of $N = 90$ discrete monomers connected by harmonic springs with contact interactions between the A and B monomers of strength χ_b. A partial saddle-point approximation was applied to the pressure field enforcing incompressibility, which facilitated the use of conventional Langevin dynamics. The results of the simulations were then mapped onto the standard Gaussian chain model (GCM) using a linear approximation, $\chi \approx z_\infty \chi_b$, for the effective Flory–Huggins parameter.

The WTMD is performed by periodically adding narrow Gaussians to a bias potential, $U(\Psi)$, at the instantaneous value, $\hat{\Psi}$, of an appropriate order parameter, Ψ. As the bias develops, the system is able to overcome the energy barrier separating the competing phases. By gradually decreasing the amplitude of the Gaussians, the system eventually reaches a well-tempered state, where the free energy as a function of the order parameter, $F(\Psi;\, \chi)$, is given by Eq. (22). Using Eq. (23), one can then calculate a histogram of the order parameter, $P(\Psi)$, which generally exhibits separate peaks for the competing phases. The phase transition can then be located by adjusting χ until the coexisting phases occur with equal probability or, in other words, until their peaks are of equal area. Provided that the simulation is run sufficiently close to the transition, the adjustment in χ can be performed using the linear extrapolation in Eq. (24).

The method worked particularly well for the lamellar–disorder transition on account of the fact that our choice of Ψ in Eq. (16) can clearly distinguish the competing phases. Given the dependence of $(\chi N)_{\mathrm{ODT}}$ on the size of the simulation box in Fig. 5, it appears that the equilibrium periodicity of an ordered phase can be adequately approximated by SCFT. Although Ψ is less effective at distinguishing the cylindrical and disordered phases, it was still able to locate the ODT. However, this was not the case for the spherical and disordered phases because of the similarity of their morphologies. Nevertheless, the WTMD was able to locate a nearby OOT between the spherical and cylindrical phases. The order parameter also struggled to distinguish the gyroid and disordered phases, which was further complicated by the presence of other metastable morphologies in the complex phase window.

The similarity between ordered and disordered phases poses a problem not just for WTMD but also for free-energy approaches. In the case of WTMD, however, this could perhaps be remedied by constructing order parameters with the help of machine learning and by employing multiple order parameters. When the order parameter is able to adequately discern the competing phases, transitions can be located with remarkable precision due to the strong dependence the histogram has on the system parameters. As such, WTMD will undoubtedly become a valuable tool in FTS.

SUPPLEMENTARY MATERIAL

See the supplementary material for the computer source code used to produce the data for this study.

ACKNOWLEDGMENTS

We are grateful to Glenn Fredrickson and Dave Morse for useful discussions. This work was supported by the NSERC of Canada, and computer resources were provided by Compute Canada.

AUTHOR DECLARATIONS

Conflict of Interest

The authors have no conflicts to disclose.

Author Contributions

Thomas M. Beardsley: Investigation (lead); Software (equal). **Mark W. Matsen:** Conceptualization (lead); Funding acquisition (lead); Methodology (lead); Software (equal); Supervision (lead); Writing – original draft (lead); Writing – review & editing (lead).

DATA AVAILABILITY

The data that support the findings of this study are available within the article and its supplementary material.

REFERENCES

[1] G. H. Fredrickson, V. Ganesan, and F. Drolet, "Field-theoretic computer simulation methods for polymers and complex fluids," Macromolecules **35**, 16–39 (2002).

[2] M. W. Matsen, "Field theoretic approach for block polymer melts: SCFT and FTS," J. Chem. Phys. **152**, 110901 (2020).

[3] M. W. Matsen and T. M. Beardsley, "Field-theoretic simulations for block copolymer melts using the partial saddle-point approximation," Polymers **13**, 2437 (2021).

[4] M. W. Matsen, "The standard Gaussian model for block copolymer melts," J. Phys.: Condens. Matter **14**, R21–R47 (2002).

[5]M. W. Matsen, "Effect of architecture on the phase behavior of AB-type block copolymer melts," Macromolecules **45**, 2161–2165 (2012).
[6]G. H. Fredrickson and E. Helfand, "Fluctuation effects in the theory of microphase separation in block copolymers," J. Chem. Phys. **87**, 697–705 (1987).
[7]T. M. Beardsley and M. W. Matsen, "Fluctuation correction for the order-disorder transition of diblock polymer melts," J. Chem. Phys. **154**, 124902 (2021).
[8]F. S. Bates, M. F. Schulz, A. K. Khandpur, S. Förster, J. H. Rosedale, K. Almdal, and K. Mortensen, "Fluctuations, conformational asymmetry and block copolymer phase behaviour," Faraday Discuss. **98**, 7–18 (1994).
[9]E. M. Lennon, K. Katsov, and G. H. Fredrickson, "Free energy evaluation in field-theoretic polymer simulations," Phys. Rev. Lett. **101**, 138302 (2008).
[10]V. Ganesan and G. H. Fredrickson, "Field-theoretic polymer simulations," Europhys. Lett. **55**, 814–820 (2001).
[11]G. H. Fredrickson and K. T. Delaney, "Direct free energy evaluation of classical and quantum many-body systems via field-theoretic simulation," Proc. Natl. Acad. Sci. U. S. A. **119**, e2201804119 (2022).
[12]M. Olvera de la Cruz, S. F. Edwards, and I. C. Sanchez, "Concentration fluctuations in polymer blend thermodynamics," J. Chem. Phys. **89**, 1704–1708 (1988).
[13]K. T. Delaney and G. H. Fredrickson, "Recent developments in fully fluctuating field-theoretic simulations of polymer melts and solutions," J. Phys. Chem. B **120**, 7615–7634 (2016).
[14]M. Takenaka, T. Wakada, S. Akasaka, S. Nishitsuji, K. Saijo, H. Shimizu, M. I. Kim, and H. Hasegawa, "Orthorhombic *Fddd* network in diblock copolymer melts," Macromolecules **40**, 4399–4402 (2007).
[15]Y.-C. Wang, K. Matsuda, M. I. Kim, A. Miyoshi, S. Akasaka, S. Nishitsuji, K. Saijo, H. Hasegawa, K. Ito, T. Hikima, and M. Takenaka, "Fddd phase boundary of polystyrene-block-polyisoprene diblock copolymer melts in the polystyrene-rich region," Macromolecules **48**, 2211–2216 (2015).
[16]E. Reister, M. Müller, and K. Binder, "Spinodal decomposition in a binary polymer mixture: Dynamic self-consistent-field theory and Monte Carlo simulations," Phys. Rev. E **64**, 041804 (2001).
[17]D. Düchs, V. Ganesan, G. H. Fredrickson, and F. Schmid, "Fluctuation effects in ternary AB + A + B polymeric emulsions," Macromolecules **36**, 9237–9248 (2003).
[18]A. Alexander-Katz and G. H. Fredrickson, "Diblock copolymer thin films: A field-theoretic simulation study," Macromolecules **40**, 4075–4087 (2007).
[19]T. M. Beardsley, R. K. W. Spencer, and M. W. Matsen, "Computationally efficient field-theoretic simulations for block copolymer melts," Macromolecules **52**, 8840–8848 (2019).
[20]T. M. Beardsley and M. W. Matsen, "Calibration of the Flory–Huggins interaction parameter in field-theoretic simulations," J. Chem. Phys. **150**, 174902 (2019).
[21]J. Qin and D. C. Morse, "Renormalized one-loop theory of correlations in polymer blends," J. Chem. Phys. **130**, 224902 (2009).
[22]J. Glaser, P. Medapuram, T. M. Beardsley, M. W. Matsen, and D. C. Morse, "Universality of block copolymer melts," Phys. Rev. Lett. **113**, 068302 (2014).
[23]P. Medapuram, J. Glaser, and D. C. Morse, "Universal phenomenology of symmetric diblock copolymers near the order-disorder transition," Macromolecules **48**, 819–839 (2015).
[24]J. Glaser, J. Qin, P. Medapuram, and D. C. Morse, "Collective and single-chain correlations in disordered melts of symmetric diblock copolymers: Quantitative comparison of simulations and theory," Macromolecules **47**, 851–869 (2014).
[25]P. Grzywacz, J. Qin, and D. C. Morse, "Renormalization of the one-loop theory of fluctuations in polymer blends and diblock copolymer melts," Phys. Rev. E **76**, 061802 (2007).
[26]J. Qin, P. Grzywacz, and D. C. Morse, "Renormalized one-loop theory of correlations in disordered diblock copolymers," J. Chem. Phys. **135**, 084902 (2011).
[27]A. Barducci, G. Bussi, and M. Parrinello, "Well-tempered metadynamics: A smoothly converging and tunable free-energy method," Phys. Rev. Lett. **100**, 020603 (2008).
[28]T. Ghasimakbari and D. C. Morse, "Order-disorder transitions and free energies in asymmetric diblock copolymers," Macromolecules **53**, 7399–7409 (2020).
[29]M. W. Matsen, "Self-consistent field theory for melts of low-molecular-weight diblock copolymer," Macromolecules **45**, 8502–8509 (2012).
[30]D. Düchs, K. T. Delaney, and G. H. Fredrickson, "A multi-species exchange model for fully fluctuating polymer field theory simulations," J. Chem. Phys. **141**, 174103 (2014).
[31]D. G. Anderson, "Iterative procedures for nonlinear integral equations," J. Assoc. Comput. Mach. **12**, 547–560 (1965).
[32]D. Yong and J. U. Kim, "Accelerating Langevin field-theoretic simulation of polymers with deep learning," Macromolecules **55**, 6505–6515 (2022).
[33]P. Stasiak and M. W. Matsen, "Monte Carlo field-theoretic simulations for melts of symmetric diblock copolymer," Macromolecules **46**, 8037–8045 (2013).
[34]B. Vorselaars, P. Stasiak, and M. W. Matsen, "Field-theoretic simulation of block copolymers at experimentally relevant molecular weights," Macromolecules **48**, 9071–9080 (2015).
[35]A. Laio and M. Parrinello, "Escaping free-energy minima," Proc. Natl. Acad. Sci. U. S. A. **99**, 12562–12566 (2002).
[36]G. Bussi and A. Laio, "Using metadynamics to explore complex free-energy landscapes," Nat. Rev. Phys. **2**, 200–212 (2020).
[37]M. W. Matsen, "Cylinder ↔ sphere epitaxial transitions in block copolymer melts," J. Chem. Phys. **114**, 8165–8173 (2001).
[38]J. D. Willis, T. M. Beardsley, and M. W. Matsen, "Calibration of a lattice model for high-molecular-weight block copolymer melts," J. Chem. Phys. **150**, 204906 (2019).
[39]J. D. Willis, T. M. Beardsley, and M. W. Matsen, "A simple and accurate method to determine the Flory–Huggins χ parameter," Macromolecules **53**, 9973–9982 (2020).
[40]R. K. W. Spencer, B. Vorselaars, and M. W. Matsen, "Continuous thermodynamic integration in field-theoretic simulations of structured polymers," Macromol. Theory Simul. **26**, 1700036 (2017).
[41]Fredrickson and Delaney[11] rescale the fields by $\sqrt{V}$ when they differentiate H_f, which is mathematically equivalent to removing F_{UV} from H_f. Furthermore, their ratio of χ/χ_b does not depend on the grid resolution, and therefore, they evaluate the derivative at constant χ_b.